RMetS

Royal Meteorological Society

Balanced and unbalanced aspects of tropical cyclone intensification

Hai Hoang Bui,[a] Roger K. Smith,[b]* Michael T. Montgomery[c,d]† and Jiayi Peng[c]

[a]*Vietnam National University, Hanoi, Vietnam*
[b]*Meteorological Institute, University of Munich, Germany*
[c]*Departtment of Meteorology, Naval Postgraduate School, Monterey, California, USA*
[d]*NOAA Hurricane Research Division, Miami, Florida, USA*

ABSTRACT: We investigate the extent to which the azimuthally–averaged fields from a three-dimensional, non-hydrostatic, tropical cyclone model can be captured by axisymmetric balance theory. The secondary (overturning) circulation and balanced tendency for the primary circulation are obtained by solving a general form of the Sawyer–Eliassen equation with the diabatic heating, eddy heat fluxes and tangential momentum sources (eddy momentum fluxes, boundary-layer friction and subgrid-scale diffusion) diagnosed from the model. The occurrence of regions of weak symmetric instability at low levels and in the upper-tropospheric outflow layer requires a regularization procedure so that the Sawyer–Eliassen equation remains elliptic. The balanced calculations presented capture a major fraction of the azimuthally–averaged secondary circulation of the three-dimensional simulation except in the boundary layer, where the balanced assumption breaks down and where there is an inward agradient force. In particular, the balance theory is shown to significantly underestimate the low-level radial inflow and therefore the maximum azimuthal-mean tangential wind tendency. In the balance theory, the diabatic forcing associated with the eyewall convection accounts for a large fraction of the secondary circulation. The findings herein underscore both the utility of axisymmetric balance theory and also its limitations in describing the axisymmetric intensification physics of a tropical cyclone vortex. Copyright © 2009 Royal Meteorological Society

1. Introduction

This is one of a series of papers investigating tropical cyclone amplification. In the first paper, Nguyen *et al.* (2008, henceforth M1) examined tropical cyclone intensification and predictability in the context of an idealized three-dimensional numerical model on an f-plane and a β-plane. The aim of the current paper is to investigate the extent to which a balanced approach is useful in understanding vortex evolution in their f-plane calculations and to examine the limitations of such a theory in general.

The Nguyen *et al.* model has relatively basic physics including a bulk-aerodynamic formulation of surface friction and a simple explicit moisture scheme to represent deep convection. In the prototype amplification problem starting with a weak, axisymmetric, tropical-storm-strength vortex, the emergent flow becomes highly asymmetric and is dominated by deep convective vortex structures, even though the problem as posed is essentially

axisymmetric. These convective elements enhance locally the already elevated rotation and are referred to as 'vortical hot towers' (VHTs), a term introduced in earlier studies by Hendricks *et al.* (2004) and Montgomery *et al.* (2006). The last two studies together with that of M1 found that the VHTs are the basic coherent structures in the vortex intensification process. A similar process of evolution occurs even in a minimal tropical cyclone model (Shin and Smith, 2008).

The second paper in the series, Montgomery *et al.* (2009, henceforth M2), explored in detail the thermodynamical aspects of the Nguyen *et al.* calculations and challenged the very foundation of the evaporation–wind feedback mechanism, which is the generally accepted explanation for tropical cyclone intensification. The third paper, Smith *et al.* (2009, henceforth M3), focussed on the dynamical aspects of the azimuthally averaged fields in the two main calculations.

A significant finding of M3 is the existence of two mechanisms for the spin-up of the mean tangential circulation of a tropical cyclone. The first involves convergence of absolute angular momentum above the boundary layer[‡] where this quantity is approximately

---

*Correspondence to: Roger K. Smith, Meteorological Institute, University of Munich, Theresienstr. 37, 80333 Munich, Germany.
E-mail: roger.smith@lmu.de
†The contribution of Michael T. Montgomery to this article was prepared as part of his official duties as a United States Federal Government employee

‡As in M3, we use the term 'boundary layer' to describe the shallow layer of strong inflow near the sea surface that is typically 500 m to

Report Documentation Page		*Form Approved* *OMB No. 0704-0188*

1. REPORT DATE **JUN 2009**	2. REPORT TYPE	3. DATES COVERED **00-00-2009 to 00-00-2009**
4. TITLE AND SUBTITLE **Balanced and unbalanced aspects of tropical cyclone intensification**		5a. CONTRACT NUMBER
		5b. GRANT NUMBER
		5c. PROGRAM ELEMENT NUMBER
6. AUTHOR(S)		5d. PROJECT NUMBER
		5e. TASK NUMBER
		5f. WORK UNIT NUMBER
7. PERFORMING ORGANIZATION NAME(S) AND ADDRESS(ES) **Naval Postgraduate School,Department of Meteorology,Monterey,CA,93943**		8. PERFORMING ORGANIZATION REPORT NUMBER
9. SPONSORING/MONITORING AGENCY NAME(S) AND ADDRESS(ES)		10. SPONSOR/MONITOR'S ACRONYM(S)
		11. SPONSOR/MONITOR'S REPORT NUMBER(S)
12. DISTRIBUTION/AVAILABILITY STATEMENT **Approved for public release; distribution unlimited**		
13. SUPPLEMENTARY NOTES		

14. ABSTRACT

We investigate the extent to which the azimuthally?averaged fields from a three-dimensional, nonhydrostatic tropical cyclone model can be captured by axisymmetric balance theory. The secondary (overturning) circulation and balanced tendency for the primary circulation are obtained by solving a general form of the Sawyer?Eliassen equation with the diabatic heating, eddy heat fluxes and tangential momentum sources (eddy momentum fluxes, boundary-layer friction and subgrid-scale diffusion) diagnosed from the model. The occurrence of regions of weak symmetric instability at low levels and in the upper-tropospheric outflow layer requires a regularization procedure so that the Sawyer?Eliassen equation remains elliptic. The balanced calculations presented capture a major fraction of the azimuthally?averaged secondary circulation of the three-dimensional simulation except in the boundary layer, where the balanced assumption breaks down and where there is an inward agradient force. In particular, the balance theory is shown to significantly underestimate the low-level radial inflow and therefore the maximum azimuthal-mean tangential wind tendency. In the balance theory, the diabatic forcing associated with the eyewall convection accounts for a large fraction of the secondary circulation. The findings herein underscore both the utility of axisymmetric balance theory and also its limitations in describing the axisymmetric intensification physics of a tropical cyclone vortex.

15. SUBJECT TERMS					
16. SECURITY CLASSIFICATION OF:			17. LIMITATION OF ABSTRACT	18. NUMBER OF PAGES	19a. NAME OF RESPONSIBLE PERSON
a. REPORT **unclassified**	b. ABSTRACT **unclassified**	c. THIS PAGE **unclassified**	**Same as Report (SAR)**	**17**	

conserved and the second involves its convergence within the boundary layer, where it is not conserved, but where air parcels are displaced farther radially inwards than air parcels above the boundary layer. The latter mechanism is associated with the development of supergradient wind speeds in the boundary layer and is one to spin up the inner core region. The former mechanism acts to spin up the outer circulation at radii where the boundary-layer flow is subgradient.

It was shown in M3 that, over much of the troposphere, the azimuthally–averaged tangential wind is in close gradient wind balance, the main exceptions being in the frictional inflow layer and, to a lesser extent, in the eyewall (Figure 6 of M3). Such a result would be largely anticipated from a scale analysis of the equations, which shows that balance is to be expected where the radial component of the flow is much less than the tangential component (Willoughby, 1979).

A scale analysis shows also that, on the vortex scale, the flow is in close hydrostatic balance. Thus in regions where gradient wind balance and hydrostatic balance prevail, the azimuthally–averaged tangential component of the flow satisfies the thermal wind equation. For the purposes of this paper we refer to this as 'the balanced state'.

The validity of gradient wind balance in the lower to middle troposphere in tropical cyclones is supported by aircraft measurements (Willoughby, 1990; Bell and Montgomery, 2008), but there is some ambiguity from numerical models. In a high-resolution (6 km horizontal grid) simulation of hurricane *Andrew* (1992), Zhang *et al.* (2001) showed that the azimuthally–averaged tangential winds above the boundary layer satisfy gradient wind balance to within a relative error of 10%, the main regions of imbalance being in the eyewall and, of course, in the boundary layer. However, in a simulation of hurricane *Opal* (1995) using the Geophysical Fluid Dynamics Laboratory (GFDL) hurricane prediction model, Möller and Shapiro (2002) found unbalanced flow extending far outside the eyewall region in the upper-tropospheric outflow layer.

The thermal wind equation relates the vertical shear of the tangential velocity component to the radial and vertical density gradients (Smith *et al.*, 2005). Where it is satisfied, it imposes a strong constraint on the evolution of a vortex that is being forced by processes such as diabatic heating or friction, processes that try to drive the flow away from balance. Indeed, in order for the vortex to remain in gradient and hydrostatic balance, a transverse, or secondary circulation is required. This circulation is determined by solving a diagnostic equation

for the streamfunction of the meridional circulation. This equation is often referred to as the Sawyer–Eliassen (SE) equation (Willoughby, 1979; Shapiro and Willoughby, 1982). For completeness, the derivation of the SE equation in a simple context is sketched in section 2. Shapiro and Willoughby (1982) derived a more general form of the SE equation based on the so-called anelastic approximation and presented some basic solutions for a range of idealized forcing scenarios such as point sources of heat and tangential momentum. More recent solutions focussing on the forced subsidence in hurricane eyes are presented by Schubert *et al.* (2007). A very general form of the thermal wind equation together with a correspondingly general form of the SE equation is given by Smith *et al.* (2005).

Early attempts to exploit the gradient-wind-balance assumption in studying hurricane intensification were those of Ooyama (1969) and Sundqvist (1970). Schubert and Hack (1983) showed that an axisymmetric balance theory for an evolving vortex could be elegantly formulated using potential radius instead of physical radius as the radial coordinate (section 2). This approach was followed by Schubert and Alworth (1987), who examined the intensification of a hurricane-scale vortex in response to a prescribed heating function near the axis of rotation. In addition to potential radius, these authors used isentropic coordinates instead of physical height, a choice that simplifies the equations even further, but this simplification comes with a cost. As pointed out by Möller and Smith (1994), the heating function prescribed by Schubert and Alworth becomes progressively distorted because it has a maximum at the vortex axis and the isentropic surfaces descend markedly near the axis as the vortex develops. Thus the heating distribution becomes more and more unrealistic vis-à-vis a tropical cyclone as the vortex intensifies. Möller and Smith showed that the deformation of the heating distribution is considerably reduced if the latter is specified in an annular region, which is more realistic at the stage when deep convection is organized in the eyewall clouds typical of a mature tropical cyclone.

It is now recognized that the prescription of an arbitrary heating function is not very realistic for a tropical cyclone. For one thing, it ignores the important constraint imposed by surface moisture fluxes. Furthermore, it ignores the fact that, to a first approximation, air rising in deep convection conserves its pseudo-equivalent potential temperature. Such conservation imposes an implicit constraint on the heating distribution along slantwise trajectories of the transverse circulation. Notwithstanding this limitation, the foregoing calculations are of fundamental interest because, unlike the prototype problem for tropical cyclone intensification discussed in M1, there is no initial vortex and a vortex forms and intensifies solely by radial convergence of the initial planetary angular momentum in the lower troposphere induced by the heating. There is no frictional boundary layer in the model. Thus the formulation isolates one important aspect of tropical cyclone intensification, namely the convergence of absolute angular momentum under conditions when this quantity is conserved.

---

1 km deep and which arises largely because of the frictional disruption of gradient wind balance near the surface. While in our model calculations there is some inflow throughout the lower troposphere associated with the balanced response of the vortex to latent heat release in the eyewall clouds (we show this later in this paper), the largest radial wind speeds are confined within the lowest kilometre and delineate clearly the layer in which friction effects are important (i.e. where there is gradient wind imbalance; Figure 6 of M3) from the region above where they are not.

The balance framework has been used also to study asymmetric aspects of tropical cyclone evolution (e.g. Shapiro and Montgomery, 1993; Montgomery and Kallenbach, 1997). One topical example concerns the interaction of a tropical cyclone with its environment, early studies being those of Challa and Pfeffer (1980) and Pfeffer and Challa (1981), and more recent ones by Persing *et al.* (2002) and Möller and Shapiro (2002). The last paper examined balanced aspects of the intensification of hurricane *Opal* (1995) as captured by the GFDL model. Using the balance framework, they sought to investigate the influence of an upper-level trough on the intensification of the storm. They diagnosed the diabatic heating and azimuthal momentum sources from azimuthal averages of the model output at selected times and solved the SE equation with these as forcing functions to determine the contributions to the secondary circulation from these source terms. Then they calculated the azimuthal-mean tendencies of the azimuthal wind component associated with these contributions for intensifying and non-intensifying phases of the storm.

In two more recent papers, Hendricks *et al.* (2004) and Montgomery *et al.* (2006) used a form of the SE equation in pseudo-height coordinates to investigate the extent to which vortex evolution in a three-dimensional cloud-resolving numerical model of hurricane genesis could be interpreted in terms of balanced, axisymmetric dynamics. Again they diagnosed the diabatic heating and azimuthal momentum sources from azimuthal averages of the model output at selected times and solved the SE equation with these as forcing functions. Then they compared the azimuthal-mean radial and vertical velocity fields from the numerical model with those derived from the streamfunction obtained by solving the SE equation. They found good agreement between the two measures of the azimuthal-mean secondary circulation and concluded that the early vortex evolution proceeded in a broad sense as a balanced response to the azimuthal-mean forcing by the three-dimensional convective structures in the numerical model. However, they called for further studies to underpin these findings. The last two studies suggest that a similar calculation could be insightful when applied to the three-dimensional calculations in M1. Indeed it might allow an assessment of the separate contributions of diabatic heating and boundary-layer friction to producing convergence of absolute angular momentum above and within the boundary layer as identified in M3 to be the two intrinsic mechanisms of spin-up in an axisymmetric framework. It would provide also an idealized baseline calculation to compare with the results of the more complicated and coarser-resolution case-studies of Persing *et al.* (2002) and Möller and Shapiro (2002). One of the primary aims of this paper is to address these issues for axisymmetric tropical cyclone dynamics.

The paper is organized as follows. In section 2 we review briefly the main features of the axisymmetric balance formulation of the hurricane intensification problem and the derivation of the SE equation. In section 3 we explain how the forcing functions for the SE equation are obtained from the MM5 calculation and in section 4 we describe the method for solving the SE equation, with special attention given to the treatment of regions that arise where the equation is ill-conditioned. Then, in section 5, we present solutions of the general form of the SE equation with the forcing functions derived from the numerical model calculations in M1. In particular, we compare these solutions with the axisymmetric mean of the numerical solutions at selected times. We study also the consequences of using the azimuthally–averaged temperature field in the formulation of the SE equation, as was done in previous studies, instead of the temperature field that is in thermal wind balance with the azimuthally–averaged tangential wind field.

2. Axisymmetric balanced hurricane models

The cornerstone of all balance theories for vortex evolution is the SE equation, which is one of a set of equations describing the slow evolution of an axisymmetric vortex forced by heat and (azimuthal) momentum sources. The flow is assumed to be axisymmetric and in strict gradient wind and hydrostatic balance. We summarize first the balance theory in a simple configuration.

2.1. A simple form of axisymmetric balance theory

Consider the axisymmetric flow of an incompressible Boussinesq fluid with constant ambient Brunt–Väisälä frequency, N. The hydrostatic primitive equations for this case may be expressed in cylindrical polar coordinates (r, λ, z) as

$$\frac{\partial u}{\partial t} + u\frac{\partial u}{\partial r} + w\frac{\partial u}{\partial z} - C = -\frac{\partial P}{\partial r} + F_r, \quad (1)$$

$$\frac{\partial v}{\partial t} + u\frac{\partial v}{\partial r} + w\frac{\partial v}{\partial z} + \frac{uv}{r} + fu = F_\lambda, \quad (2)$$

$$0 = -\frac{\partial P}{\partial z} + b, \quad (3)$$

$$\frac{\partial b}{\partial t} + u\frac{\partial b}{\partial r} + w\frac{\partial b}{\partial z} + N^2 w = \dot{B}, \quad (4)$$

$$\frac{\partial ru}{\partial r} + \frac{\partial rw}{\partial z} = 0, \quad (5)$$

where r, λ, z are the radial, azimuthal and vertical coordinates, respectively, (u, v, w) is the velocity vector in this coordinate system, $C = v^2/r + fv$ is the sum of the centrifugal and Coriolis terms, $P = p/\overline{\rho}$ is the pressure p divided by the mean density $\overline{\rho}$ at height z, b is the buoyancy force, defined as $-g\{\rho - \overline{\rho}(z)\}/\rho^*$, where ρ is the density, ρ^* is the average density over the whole domain, $\dot{B}$ is the diabatic source of buoyancy, and F_r and F_λ are the radial and tangential components of frictional stress, respectively.

With the additional assumption of strict gradient wind balance, Equation (1) reduces to

$$C = \frac{\partial P}{\partial r}. \quad (6)$$

If P is eliminated from this equation by cross-differentiation with the hydrostatic equation, Equation (3), we obtain the thermal wind equation

$$\frac{\partial b}{\partial r} = \xi \frac{\partial v}{\partial z}, \tag{7}$$

where $\xi = 2v/r + f$ is twice the absolute angular velocity. The SE equation is obtained by differentiating Equation (7) with respect to time, eliminating the time derivatives of v and b using Equations (2) and (4) and introducing a streamfunction ψ for the secondary circulation such that the continuity Equation (5) is satisfied, i.e. we write $u = -(1/r)(\partial\psi/\partial z)$ and $w = (1/r)(\partial\psi/\partial r)$. Then, with a little algebra we obtain:

$$\frac{\partial}{\partial r}\left[\left(N^2 + \frac{\partial b}{\partial z}\right)\frac{1}{r}\frac{\partial\psi}{\partial r} - \frac{S\xi}{r}\frac{\partial\psi}{\partial z}\right]$$
$$+ \frac{\partial}{\partial z}\left[\frac{\xi\zeta_a}{r}\frac{\partial\psi}{\partial z} - \frac{\xi S}{r}\frac{\partial\psi}{\partial r}\right]$$
$$= \frac{\partial\dot{B}}{\partial r} - \frac{\partial}{\partial z}(\xi F_\lambda), \tag{8}$$

where $S = \partial v/\partial z$ is the vertical wind shear and $\zeta_a = (1/r)(\partial rv/\partial r) + f$ is the absolute vorticity. More general derivations of this equation are found, for example, in Willoughby (1979), Shapiro and Willoughby (1982) and Smith *et al.* (2005).

The SE equation is elliptic if the vortex is symmetrically stable (i.e. if the inertial stability on isentropic surfaces is greater than zero). It is readily shown that symmetric stability is assured when

$$\left(N^2 + \frac{\partial b}{\partial z}\right)\zeta_a\xi - (\xi S)^2 > 0$$

(Shapiro and Montgomery, 1993). Given suitable boundary conditions, this equation may be solved for the streamfunction, ψ, at a given time. Being a balanced model, only one prognostic equation is used to advance the system forward in time. The set of Equations (2), (7) and (8) thus provide a system that can be solved for the balanced evolution of the vortex. Equation (2) along with the thermal wind Equation (7)[§] is used to predict the future state of the primary circulation with values of u and w at a given time being computed from the streamfunction ψ obtained by solving Equation (8). The secondary circulation given by Equation (8) is just that required to keep the primary circulation in hydrostatic and gradient wind balance in the presence of the processes trying to drive it out of balance. These processes are represented by the radial gradient of the rate of buoyancy generation and the vertical gradient of ξ times the tangential component of frictional stress. It follows that surface friction *can* induce radial motion in a balanced

formulation of the boundary layer, although the balanced assumption is not generally valid in this layer (Smith and Montgomery, 2008).

The SE equation can be simplified by using potential radius coordinates in which the radius, r, is replaced by the potential radius, R, defined by $fR^2/2 = rv + fr^2/2$, the right-hand side being the absolute angular momentum (Schubert and Hack, 1983). Physically, the potential radius is the radius to which an air parcel must be moved (conserving absolute angular momentum) in order to change its relative angular momentum, or equivalently its azimuthal velocity component, to zero. With this coordinate, surfaces of absolute angular momentum are vertical and the assumption that these surfaces are coincident with the moist isentropes provides an elegant way to formulate the zero-order effects of moist convection (Emanuel, 1986, 1989, 1995a, b, 1997, 2003). However it is not clear how to incorporate an unbalanced boundary layer into such a formulation and there are additional difficulties when the vortex becomes inertially unstable.

2.2. General form of axisymmetric balance theory

The Boussinesq approximation in height coordinates is generally too restrictive for flow in a deep atmosphere, but it is possible to formulate the SE equation without making any assumptions on the smallness of density perturbations. A very general version of the thermal wind equation that assumes only that the flow is in hydrostatic and gradient wind balance was given by Smith *et al.* (2005):

$$g\frac{\partial}{\partial r}\ln\rho + C\frac{\partial}{\partial z}\ln\rho = -\xi\frac{\partial v}{\partial z}. \tag{9}$$

It turns out to be convenient to define $\chi = 1/\theta$, where θ is the potential temperature, whereupon Equation (9) becomes

$$g\frac{\partial\chi}{\partial r} + \frac{\partial(\chi C)}{\partial z} = 0, \tag{10}$$

and the thermodynamic equation can be recast as

$$\frac{\partial\chi}{\partial t} + u\frac{\partial\chi}{\partial r} + w\frac{\partial\chi}{\partial z} = -\chi^2 Q, \tag{11}$$

where Q is the diabatic heating rate for the azimuthally–averaged potential temperature. Again taking the time derivative of the thermal wind equation and eliminating the time derivatives using the tangential momentum and thermodynamic equations leads to a diagnostic equation for the secondary circulation. The continuity equation is now

$$\frac{\partial}{\partial r}(\rho r u) + \frac{\partial}{\partial z}(\rho r w) = 0, \tag{12}$$

and implies the existence of a streamfunction ψ satisfying

$$u = -\frac{1}{r\rho}\frac{\partial\psi}{\partial z}, \qquad w = \frac{1}{r\rho}\frac{\partial\psi}{\partial r}. \tag{13}$$

[§]Note that knowledge of v enables Equation (7) to be solved under all circumstances using the method described by Smith (2006). However, given the thermal field characterized by b, it is not always possible to find a corresponding balanced wind field, v.

With a little algebra, the SE Equation (14) follows by substituting for u and w in the foregoing diagnostic equation and using the thermal wind relationship together with the definitions of C, ξ and ζ.

The streamfunction, ψ, for the toroidal overturning circulation forced by the distributions of diabatic heating and frictional torque, analogous to Shapiro and Willoughby's Equation (5), but consistent with the thermal wind Equation (9) is now:

$$\frac{\partial}{\partial r}\left[-g\frac{\partial \chi}{\partial z}\frac{1}{\rho r}\frac{\partial \psi}{\partial r} - \frac{\partial}{\partial z}(\chi C)\frac{1}{\rho r}\frac{\partial \psi}{\partial z}\right]$$
$$+ \frac{\partial}{\partial z}\left[\left(\xi\chi(\zeta+f)+C\frac{\partial \chi}{\partial r}\right)\frac{1}{\rho r}\frac{\partial \psi}{\partial z} - \frac{\partial}{\partial z}(\chi C)\frac{1}{\rho r}\frac{\partial \psi}{\partial r}\right]$$
$$= g\frac{\partial}{\partial r}(\chi^2 Q) + \frac{\partial}{\partial z}(C\chi^2 Q) - \frac{\partial}{\partial z}(\chi\xi F_\lambda), \qquad (14)$$

where $\xi = 2v/r + f$ is twice the local absolute angular velocity and $\zeta = (1/r)\{\partial(rv)/\partial r\}$ is the vertical component of relative vorticity (see Appendix).

Equation (14) shows that the buoyant generation of a toroidal circulation is closely related to the curl of the rate of generation of generalized buoyancy, defined approximately in this case as $\mathbf{b} = -\mathbf{g}_e(\theta - \theta_a)/\theta_a$, where $\mathbf{g}_e = (C, -g)$ is the generalized gravitational acceleration and θ_a is the value of θ at large radius¶. The approximation is based on replacing $1/\theta$ and $1/\theta_a$ by some global average value, $1/\Theta$, as in the anelastic approximation (Ogura and Phillips, 1962). With this approximation, the term $C\partial \chi/\partial r$ in the second square bracket of Equation (14) is zero.

We note that Equation (14) is an elliptic partial differential equation provided that the discriminant

$$D = -g\frac{\partial \chi}{\partial z}\left(\xi\chi(\zeta+f)+C\frac{\partial \chi}{\partial r}\right) - \left[\frac{\partial}{\partial z}(\chi C)\right]^2 \qquad (15)$$

is positive. With a few lines of algebra, one can show that $D = g\rho\xi\chi^3 P$, where

$$P = \frac{1}{\rho\chi^2}\left(\frac{\partial v}{\partial z}\frac{\partial \chi}{\partial r} - (\zeta+f)\frac{\partial \chi}{\partial z}\right)$$

is the Ertel potential vorticity (Shapiro and Montgomery, 1993).

Smith *et al.* (2005) show that the SE equation is the time derivative of the toroidal vorticity equation in which the time rate of change of the material derivative of potential toroidal vorticity, $\eta/(r\rho)$, is set to zero. (Here $\eta = \partial u/\partial z - \partial w/\partial r$ is the toroidal (or tangential) component of relative vorticity.)

¶Normally the ambient value is taken at the same height, but for a rapidly rotating vortex such as a tropical cyclone, where the isobars dip down near the centre, it is more appropriate to take it on the same isobaric surface (Smith *et al.*, 2005).

3. Specification of the forcing functions, F_λ and $\dot\theta$

As noted earlier, the aim of this paper is to examine the balanced response of a tropical-cyclone-scale vortex by solving the SE equation with appropriate forcing functions, F_λ and $\dot\theta$. In this paper these forcing functions are nomenclature for the sum of azimuthally–averaged tangential eddy-momentum fluxes, surface friction and subgrid-scale diffusion tendencies:

$$F_\lambda = -\overline{u'\zeta'} - \overline{w'\frac{\partial v'}{\partial z}} + \overline{PBL} + \overline{DIFF} \qquad (16)$$

and azimuthally averaged eddy heat fluxes and mean diabatic heating rate:

$$Q = \overline{\dot\theta} - \overline{u'\frac{\partial\theta'}{\partial r}} - \overline{\frac{v'}{r}\frac{\partial\theta'}{\partial\lambda}} - \overline{w'\frac{\partial\theta'}{\partial z}} + \overline{DIFH} \qquad (17)$$

respectively, where $\dot\theta$ is the total diabatic heating rate. Here an overbar denotes an azimuthal average, a prime denotes a deviation therefrom, *PBL* denotes planetary boundary layer for tangential momentum (in this case bulk aerodynamic drag), ζ' denotes the eddy vertical vorticity, *DIFF* and *DIFH* denote the subgrid-scale diffusion of tangential momentum and heat, and λ is the azimuthal angle. These forcing functions were diagnosed at selected times from the control calculation in M1, which is one of the idealized, three-dimendional calculations of tropical cyclone intensification using the MM5 model discussed in that paper. Figure 1 shows a time series of maximum azimuthally–averaged tangential wind speed at 900 hPa in this calculation. After a brief gestation period during which the boundary layer becomes established and moistened by the surface moisture flux, the vortex rapidly intensifies before settling down into a quasi-steady state (albeit with some fluctuations in intensity).

The forcing functions defined above are obtained as follows. The MM5 output data are extracted at 15 min intervals and converted into pressure coordinates. The
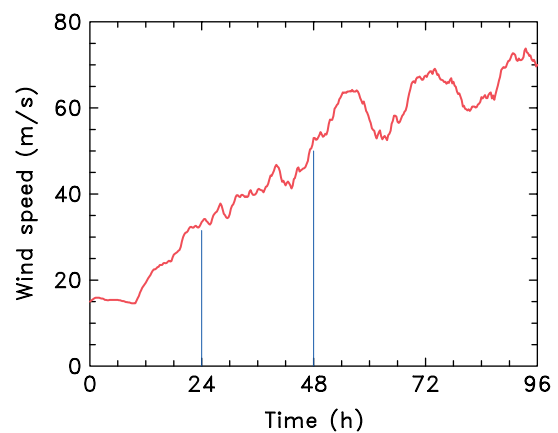

Figure 1. Time series of maximum azimuthally–averaged tangential wind speed at 900 hPa in the control calculation of Nguyen *et al.* (2008), on which the calculations here are based. The two vertical lines indicate the two times during the period of rapid intensification for which the calculations here are carried out. This figure is available in colour online at www.interscience.wiley.com/journal/qj

surface friction and horizontal diffusion terms are output directly from the MM5 model also. The vortex centre is calculated using the same method as in M1[‖]. All variables are then transformed into cylindrical polar coordinates. Pertinent fields, including the eddy heat and eddy momentum fluxes noted above, are azimuthally averaged about the identified centre. The azimuthal mean data are interpolated linearly into height coordinates with a vertical grid spacing of 500 m. Other variables (density, potential temperature and diabatic heating) are calculated from the MM5 diagnostic tool, RIP. As an approximate check on the consistency of the diabatic heating term using RIP, the heating term was calculated directly from the material rate-of-change of potential temperature using centred space and time differences (with 15 min output interval) and the results were found to be virtually identical to the corresponding calculation of the heating rate using RIP.

As found in previous work (Möller and Shapiro, 2002, section 2; Montgomery *et al.*, 2006, p 381), the eddy heat and eddy momentum flux, friction and subgrid-scale diffusion forcing terms implicit in Equation (14) are approximately an order of magnitude smaller than the corresponding forcing terms arising from the radial and vertical gradient of the azimuthally–averaged diabatic heating rate, and in the upper-tropospheric outflow layer in Möller and Shapiro's case-study where they are influenced by the large-scale environment. However, this is not to say that eddy processes are unimportant. In fact, we have shown recently that the eddies in the form of the VHTs are crucial, as they are the structures within which the local buoyancy is manifest to drive the intensification process (M1 and M2).

4. Solution of the SE equation

When the ellipticity condition, $D > 0$, is met at every grid point, the SE equation, Equation (14), can be solved using several numerical methods. The equation is first expressed as a finite-difference approximation with radial and vertical grid spacings of 5 km and 500 m, respectively. In this study, the matrix equations that result are solved using the successive overrelaxation scheme described by Press *et al.* (1992). To solve the equation, we need the value of the streamfunction on the boundary. An obvious choice at the upper and lower boundaries as well as at the axis is to take the normal velocity to be zero, equivalent to taking the streamfunction to be zero. For a large domain with a radius on the order of 1000 km, it would be probably sufficient to take a condition of zero normal flow at this boundary. However, for the 250 km domain used here it seems preferable to use a zero radial gradient condition, which constrains the vertical velocity to be zero at this boundary. Therefore, we require the streamfunction at the outer radius to satisfy $\partial \psi / \partial r = 0$. The overrelaxation parameter has

a fixed value of 1.8. The solution is deemed to be attained when the absolute error in the discretized form of Equation (14) is less than the prescribed value 10^{-24}.

The azimuthal-mean tangential wind and temperature fields obtained from the MM5 output do not satisfy the ellipticity condition at some grid points and this can affect the solution or even render the solution unobtainable. Thus a regularization procedure must be carried out to restore the ellipticity at these grid points. Here we follow the *ad hoc*, but physically defencible, method suggested by Möller and Shapiro (2002). Typically, there are two regions in which the ellipticity condition is violated: one is near the lower boundary, where $\partial(\chi C)/\partial z$ is large, and the other is in the outflow layer where the parameter, $I^2 = \chi \xi(\zeta + f) + C \partial \chi / \partial r$, which is an analogue to the inertial stability parameter of the Boussinesq system, $\xi(\zeta + f)$, is negative. The regularization process first checks the value of I^2 over the whole domain and determines its minimum value. If this value is less than or equal to zero, a small value is then added to I^2 to make sure that this value is slightly greater than zero everywhere. The value added is typically three orders of magnitude smaller than the maximum value of I^2 so that the procedure does not affect the general characteristics of the solution outside the regions where the regularization is applied. Then, if D still less than or equal to zero, S is multiplied by 0.8 of its local value at all grid points in the region where $D < 0$. As discussed in Möller and Shapiro (2002, section 2), this method does not change the basic vortex structure and makes a minimal alteration of the stability parameters so as to furnish a convergent solution.

When the ellipticity condition is well met everywhere, the solution converges to within an absolute error of 10^{-24} after about 1000 iterations. If the SE equation is solved for the streamfunction without peforming the regularization, the convergence is slower, requiring, for example at 48 h, more than 6000 iterations to meet an error criterion of 10^{-16}, or there there may be regions where the error slowly grows.

4.1. The two balanced calculations

The two main solutions of the SE equation discussed below use forcing functions, F_λ in Equation (2) and $\dot{\theta}$ in Equation (11), obtained from the MM5 control simulation in M1 as described in section 3, at two times: 24 h and 48 h. From Figure 1, these times are seen to be during the period of rapid intensification of the vortex. Figure 2 shows the azimuthally–averaged tangential wind field taken from the MM5 control simulation in M1 at 24 h and 48 h together with the corresponding *balanced* potential temperature fields at these times. The latter are obtained using the method described by Smith (2006). The figure shows also the deviation of the balanced potential temperature from its ambient value. Note that, at both times, the maximum wind speed occurs at a very low level, below 1 km. The temperature fields show a warm-core structure with maximum temperature deviations on the axis of more than 2 K at 24 h and more than 5 K at 48 h, these maxima occurring in the upper
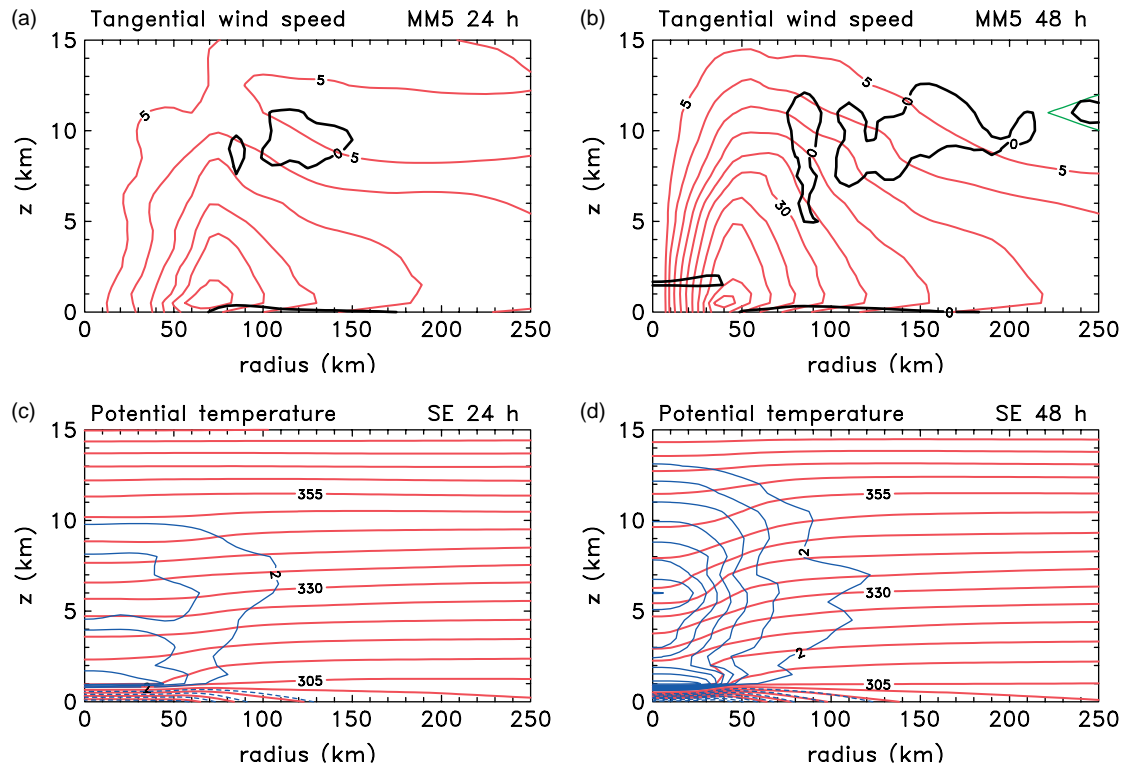

[‖]The centre is found using the location of zero wind speed at 900 hPa as the first guess, then using the vorticity centroid at 900 hPa as the next iteration.

Figure 2. Radius–height sections of isotachs of the azimuthally–averaged tangential wind component (contour interval 5 m s^{-1}) diagnosed from the three-dimensional MM5 calculation at (a) 24 h, and (b) 48 h. The thin triangular-shaped contour at the top right in (b) is the zero contour. The solid black curves enclose regions where the ellipticity condition for solving the SE equation is violated (i.e. they are the zero contour of D). (c) and (d) show the corresponding balanced potential temperature fields at these times (with contour interval 5 K), with the thin contours showing the balanced potential temperature deviation from its ambient value (contour interval 2 K for positive deviations (solid) and 4 K for negative deviations (dashed)). This figure is available in colour online at www.interscience.wiley.com/journal/qj

troposphere. At very low levels, the balanced temperature field has a cold-cored structure consistent with the increase with height of the tangential wind component near the surface. This cold-cored structure is not a feature of the azimuthally–averaged fields and arizes because the flow at these levels is *not* in close gradient-wind balance (Smith and Montgomery, 2008; M3 Figure 6).

Three options would seem to be available to address the matter of unbalanced flow: (a) to continue with the balanced potential temperature field so that the SE problem is formulated consistently as a true balance model; (b) to work with the azimuthally–averaged potential temperature field and calculate the tangential wind field that is in balance with it; or (c) to work with the azimuthally–averaged tangential wind and potential temperature fields (as in Persing and Montgomery, 2003), recognizing that they will not be exactly in balance. Option (b) has a major problem relating to the fact that, given the mass-field distribution, i.e. the radial pressure gradient, it is not always possible to calculate a corresponding balanced wind field (see footnote in section 2.1) and an *ad hoc* definition of balanced wind is necessary where a real-valued solution is non-existent. The difficulty occurs of course in regions where the vortex becomes symmetrically unstable, as happens in certain regions of the MM5 calculations (such as in the widespread upper-tropospheric outflow region of the vortex). The choice of

option (c) is accompanied by the uncertainty surrounding the lack of balance in the SE equation, an issue that is discussed in more detail in the Appendix. For these reasons, we have elected to choose the simplest option (a).

The azimuthally–averaged diabatic heating rate and tangential momentum source derived from the MM5 calculation at 24 and 48 h are shown in Figure 3. At 24 h, the diabatic heating rate is confined largely to a vertical column in an annular region with radii between 50 and 70 km. The maximum heating rate is about 20 K h^{-1} and occurs at about 6 km in altitude. At 48 h the heating rate covers a broader annulus and has two maxima, one near a radius of 48 km and the other near a radius of 65 km. The latter has the largest magnitude of 21 K h^{-1} and occurs at 6 km in altitude.

At both times there is a sink of tangential momentum in a shallow surface-based layer that is clearly attributable to the effects of surface friction. At 24 h the maximum deceleration is about 20 m s^{-1}h^{-1} and at 48 h about 50 m s^{-1}h^{-1}. This sink is stronger at 48 h because the tangential wind is stronger at this time. In the upper troposphere there is a localized tangential momentum sink also that aligns with the eyewall updraught (Figure 7 below). This feature has been traced to originate primarily from the action of eddy momentum fluxes in the eyewall associated with the VHTs. The maximum value exceeds 10 m s^{-1}h^{-1} at both times, but, as shown below, the
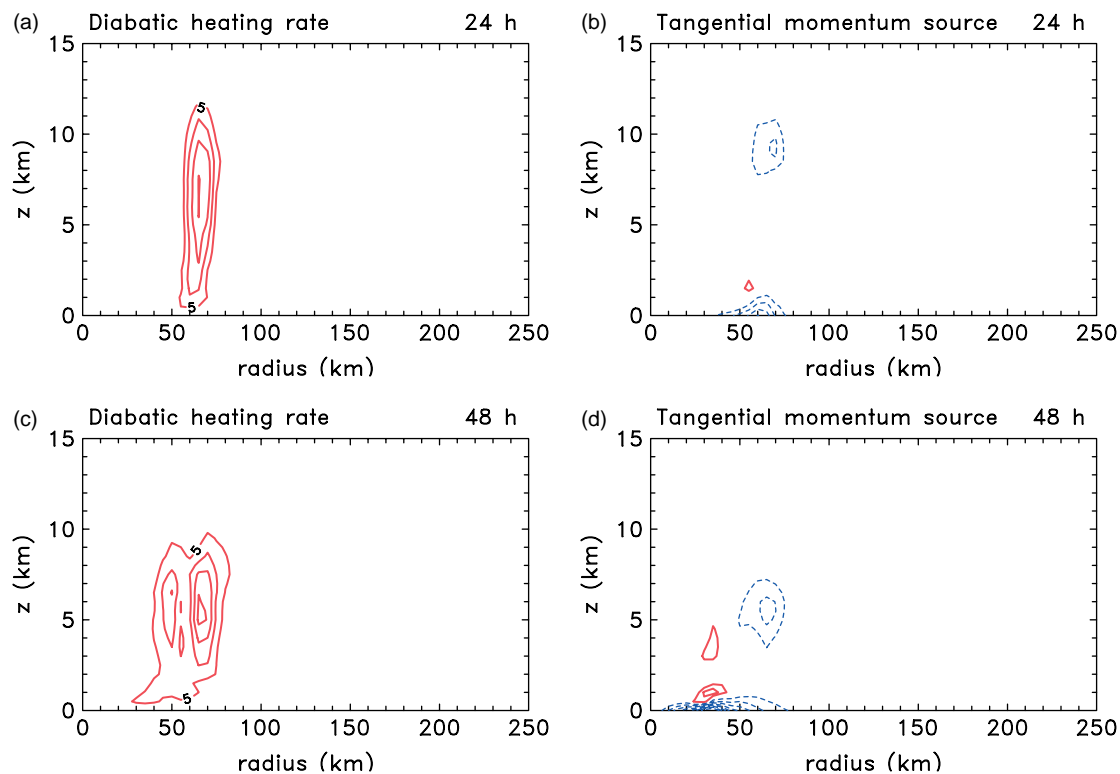
Figure 3. Radius–height sections at 24 h of (a) the azimuthally–averaged heat source (contour interval 5 K h^{-1}), and (b) the azimuthally–averaged tangential momentum source diagnosed from the three-dimensional MM5 calculation (contour interval 5.0 m s^{-1}h^{-1}, with positive contours solid and negative contours dashed). The corresponding source terms at 48 h are shown in (c) and (d). Note that the maximum momentum sink in (d) is 50 m s^{-1}h^{-1}. This figure is available in colour online at www.interscience.wiley.com/journal/qj

Figure 4. The meridional streamfunction from the solution of the Sawyer–Eliassen equation forced with the heat and momentum sources diagnosed from MM5 at (a) 24 h, and (b) 48 h, (c) with the heat source alone at 48 h, and (d) with the momentum source alone at 48 h. In (a)–(c), the contour interval is 1.0×10^6 m^{2}s^{-1} for positive values (thick solid curves) and 0.25×10^6 m^{2}s^{-1} for negative values (thin dashed curves). In (d), all intervals are 0.25×10^6 m^{2}s^{-1}. This figure is available in colour online at www.interscience.wiley.com/journal/qj

overall effect of the feature on the total solution is localized and relatively small.

5. Results

Figure 4(a) and (b) show the meridional streamfunction obtained from the solution of the SE Equation (14) with the diabatic heating rates and tangential momentum source/sinks shown in Figure 3. At both times there are two cells of circulation: an in-up-and-out cell at radii within and outside the heating source, and a cell with subsidence at radii inside the source. The inner cell has subsidence at the vortex axis and corresponds with the model 'eye'. This cell is slightly stronger at 24 h than at 48 h and extends to lower levels, consistent with the idea that the subsidence in the 'eye' is strongest during the most rapid development phase of the storm (e.g. Willoughby, 1979; Smith, 1980). In contrast, the outer cell is stronger at 48 h (see below).

Figure 4(c) and (d) show the separate contributions to the meridional streamfunction pattern from the diabatic heating rate and tangential momentum source/sink at 48 h. Comparison of (c) with (b) shows that the diabatic heating accounts for a significant fraction of the circulation, although the latter is strengthened by friction, in the balanced calculation at least, as is evidenced, for example, in the difference in the number of contours inside the contour labelled 6.0 in these panels. By itself, friction would lead to a shallow layer of outflow just above the boundary layer (Figure 4(d)), a result already shown by Willoughby (1979). This outflow is more than offset by the convergence produced by diabatic heating (Smith, 2000). It should be remembered, however, that the frictional contribution to the inflow obtained from the SE equation is based on the assumption that the boundary layer is in gradient balance, which is formally not justified (Smith and Montgomery, 2008). The consequences are very significant when one compares the balanced and unbalanced radial wind fields, which are discussed below (cf. Figures 6(a) and (b)). The localized tangential momentum sink that aligns with the eyewall updraught produces a localized circulation with inflow below it and outflow above. The effect is to elevate the streamfunction maximum and to strengthen it slightly (cf. Figures 4(b) and (c)).

Figure 5 compares the azimuthally–averaged radial and vertical wind structure in the MM5 calculation with those derived from the SE streamfunction at 24 h. It is noteworthy that the *low-level radial inflow* is significantly larger in the MM5 calculation, a feature that can be attributed to the inward agradient force in the boundary layer resulting from the reduction of the centrifugal and Coriolis forces in that layer (Figure 6(a) in M3). In the SE calculation, the centrifugal and Coriolis forces are assumed to be in balance with the radial pressure gradient. The stronger low-level inflow in the MM5 calculation is accompanied by a region of stronger outflow immediately above it, while in the balanced calculation the deep inflow above the friction layer is

stronger than in the MM5 calculation (Figure 5(e)). The vertically-integrated lower-tropospheric inflow is slightly larger in the MM5 calculation and is manifest in a marginally stronger updraught than in the balanced calculation and also in stronger subsidence near the rotation axis (cf. Figures 5(c), (d) and (f)). Moreover, the updraught extends a little higher at this time, a fact that is most likely associated with the fact that the balanced calculation assumes hydrostatic balance, an assumption that cannot represent the effects of local buoyancy in the VHTs of the MM5 calculation. (M2 provides details of the local buoyancy calculations.) In the outflow layer, the situation is reversed, with the maximum radial wind speed in the upper-level outflow being a little stronger in the balanced calculation than in the MM5 calculation. This result is consistent with the more rapid collapse of the updraught in the balanced solution. There are two outflow maximum in the balanced solution, the lower one of which is associated with the elevated tangential momentum sink seen in Figure 3(b), a feature that is discussed above. However, this feature is not obvious at this instant** in the corresponding MM5 solution.

Figures 6 and 7 compare radius–height cross-sections of the azimuthally–averaged radial wind and vertical velocity in the MM5 calculation with those derived from the SE streamfunction at 48 h. They show also the separate contributions from the effects of diabatic heating and friction. The situation is similar to that at 24 h. Again the low-level radial inflow is significantly larger in the MM5 calculation, while the inflow in the lower troposphere is stronger in the balanced calculation as at 24 h, a feature that is more evident in Figure 8(a). Again, the net inflow is similar in both calculations and the maximum vertical velocity is only a little larger in the MM5 calculation (cf. Figures 7(a) and (b)). Even so, the vertical velocity profiles at an altitude of 7 km, the approximate level of nondivergence in Figure 8(a), are almost the same (Figure 8(b)). The balanced calculation underestimates the subsidence both inside and outside the eye region, a result that is probably related to the presence of inertia-gravity waves in the MM5 calculation. Such waves are a prominent feature in animations of the vertical velocity fields and, for this reason, comparison with the instantaneous MM5 fields provides a stringent test of the balance theory. The maximum strength of the upper-troposphere outflow is similar in both calculations (cf. Figures 6(a) and (b)), but the vertical distribution is a little different as exemplified by the radial profiles in Figure 8(a). At this time, the elevated tangential momentum sink seen in Figure 3(d) does have a small signature of inflow between 4 and 5 km in height. This signature is apparent both in the balanced solution and in the MM5 solution (Figure 6(a) and (b)).

Note that the buoyant forcing normal to the lower boundary produced by the diabatic heating acts to produce an inflow layer even in the absence of friction (cf. Figure 6(c)), but this layer is deeper than that produced

---

**When diagnosing these small-scale features, one should keep in mind that the MM5 solution includes transient inertia-gravity waves.
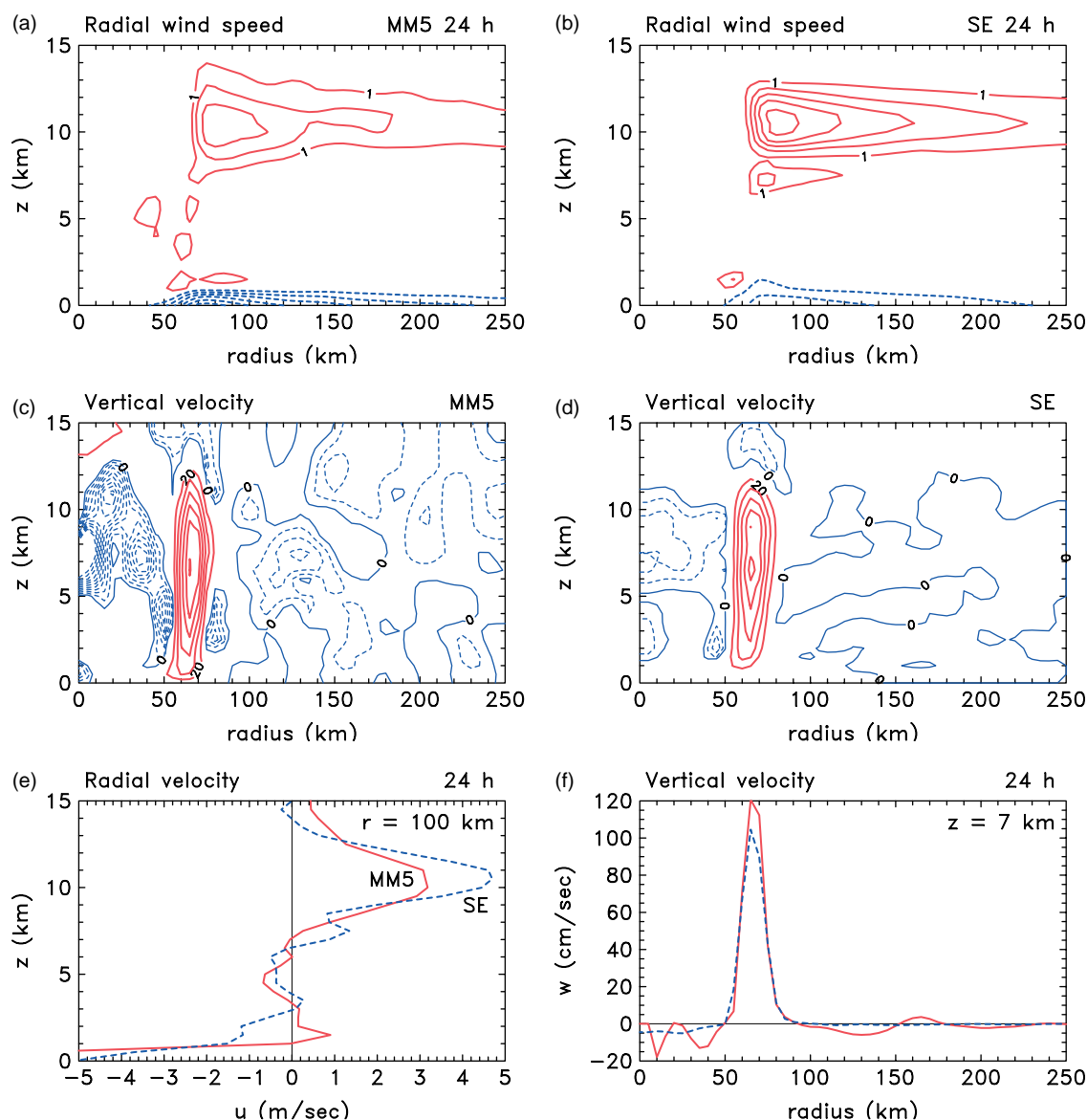
Figure 5. Radius–height cross-sections comparing isotachs of the azimuthally–averaged radial velocity, u, at 24 h (a) in the MM5 calculation, and (b) obtained from the SE streamfunction in Figure 4(a). The contour interval is 1 m s^{-1} for positive (solid) values, and 2 m s^{-1} for negative (dashed) values. (c) and (d) compare the corresponding cross-sections of azimuthally–averaged vertical velocity, w, with contour interval 20 cm s^{-1} for positive (solid) values, and 10 cm s^{-1} for negative (dashed) values. (e) compares the vertical profiles of u at a radius of 100 km in the MM5 (solid) and SE (dashed) calculations at 24 h, and (f) compares the radial profiles of w at an altitude of 7 km in these calculations. This figure is available in colour online at www.interscience.wiley.com/journal/qj

by friction alone (cf. Figure 6(d)). During the rapid intensification stage exemplified by the fields at 24 h and 48 h analysed here, the low-level inflow is greatly underestimated by the balanced calculation.

At this point it is instructive to examine the various contributions to the tendency of the azimuthally–averaged tangential wind component at low altitudes in the inner core region of the vortex, which, using Equation (2), can be written in the form:

$$\frac{\partial v}{\partial t} = -u\left(\frac{\partial v}{\partial r} + \frac{v}{r} + f\right) - w\frac{\partial v}{\partial z} + F_\lambda. \quad (18)$$

Figures 9(a)–(d) show the total influx tendency (the first two terms on the right-hand side of Equation (18)) calculated directly from the MM5 solution and from the

balanced solution at 24 and 48 h. While the overall features are similar at each time, there is a striking difference in magnitude, the MM5 tendencies being much larger than in the balanced calculation. These differences reflect the inability of the balanced calculation to fully capture the dynamics of the boundary layer in this region and especially the strength of the inflow (Figure 5). The first and second terms on the right-hand side of this equation represent contributions to the tendency from the horizontal advection of absolute vorticity (or, equivalently, the radial advection of absolute angular momentum divided by radius) and the vertical advection of tangential momentum. Figures 9(e)–(h) show centred finite-difference approximations to these two contributions at 48 h with u and w derived from the MM5
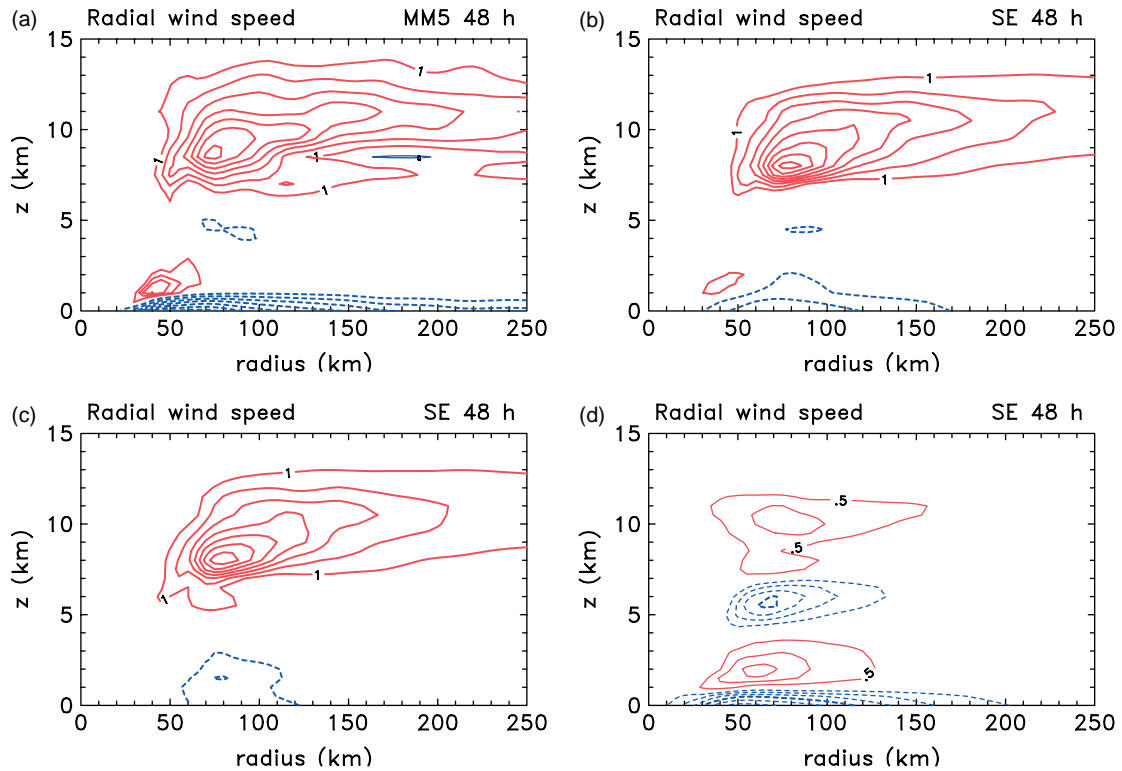
Figure 6. Radius–height sections comparing isotachs of the azimuthally–averaged radial velocity at 48 h in (a) the MM5 calculation, and (b)–(d) the corresponding ones obtained from the Sawyer–Eliassen streamfunction in Figures 4(b)–(d). In (a)–(c), the contour interval is 1 m s^{-1} for positive (solid) values, 2 m s^{-1} for negative (dashed) values. The zero contour is not plotted, and the thin line in (a) has the value -0.5 m s^{-1}. In (d) the thin contours have a spacing of 0.5 m s^{-1}. This figure is available in colour online at www.interscience.wiley.com/journal/qj
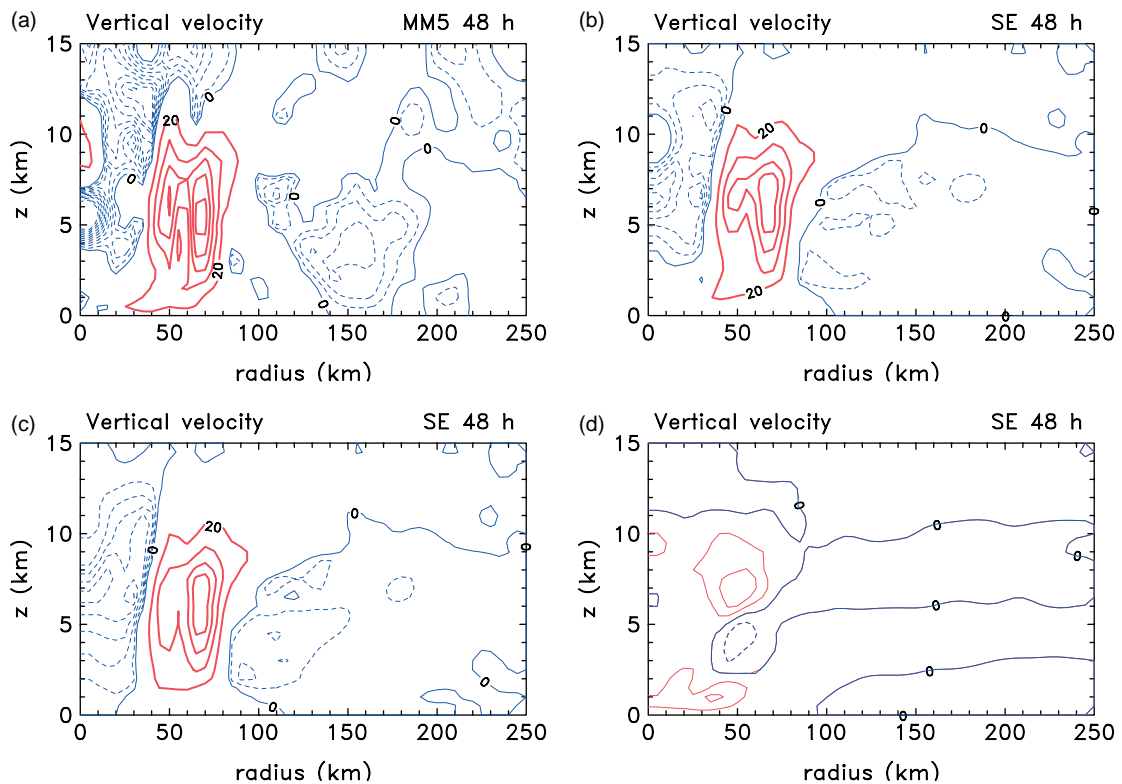

Figure 7. Radius–height cross-sections of the azimuthally–averaged vertical velocity component at 48 h in (a) the MM5 calculation, and (b)–(d) the corresponding ones obtained from the Sawyer-Eliassen-streamfunction in Figures 4(b)–(d). In (a)–(c), the contour interval is 20 cm s^{-1} for positive (solid) values and 2 cm s^{-1} for negative (dashed) values. In (d), the contour spacing is 5 cm s^{-1}). This figure is available in colour online at www.interscience.wiley.com/journal/qj
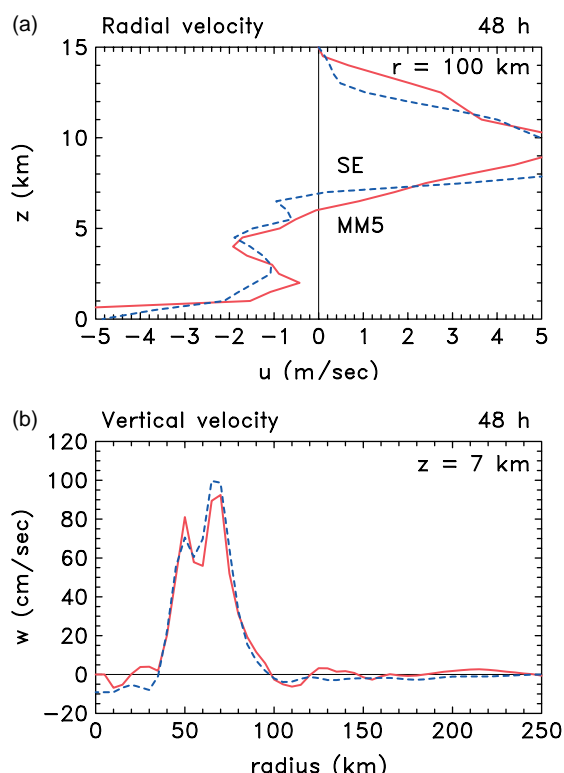
Figure 8. (a) Vertical profiles of radial velocity, u, at a radius of 100 km in the MM5 (solid curves) and SE (dashed curves) calculations at 48 h. The MM5 profiles are based on an average over 15 min intervals from 47 to 49 h. (b) Radial profiles of vertical velocity, w, at an altitude of 7 km in the MM5 (solid curves) and SE calculations (dashed curves) at 48 h. This figure is available in colour online at www.interscience.wiley.com/journal/qj

calculation (Figures 9(e) and (g)) or from the stream-function obtained from the SE equation (Figures 9(f) and (h)). The low-level tendency maxima in (c) and (d) are seen to be associated primarily with the radial influx of absolute vorticity shown in (e) and (f), respectively. This advective tendency is opposed, of course, by the negative tendency of boundary-layer friction, the distribution of which at 48 h is shown in the lower part of Figure 3(d). For this reason, the actual tendencies are much smaller than those indicated in Figure 9[††]. Since the tangential wind field in the two tendency contributions (i.e. from MM5 and SE) is the same, the differences between the contributions based on the MM5 calculation and on the balanced calculation simply reflect the different strengths of the secondary circulation, which is larger in the MM5 calculation on account of the stronger frictional inflow in the core region.

The spin-up of the eyewall is associated with the vertical advection of tangential momentum (not shown).

[††]The tendency associated with radial advection in Figure 9(e) is similar to that averaged over the period 47–49 h shown in Figure 8(b) of M3 and should be compared with Figure 8(d) of that article, which shows the total tendency for the same period, including the frictional contribution. In this case the maximum total tendency is more than an order of magnitude less than the maximum advective tendency.

This tendency is partly opposed by the negative tendency due to the radial advection of absolute vorticity because of the outward component of flow in the eyewall. Of course, this is just another way of saying that, from an axisymmetric perspective, absolute angular momentum is conserved as air parcels move upwards and outwards. Application of the axisymmetric balanced model to the rapid intensification of hurricane *Opal* in 1995 found that the balanced tendency in the eyewall region above the boundary layer was too large by a factor of two compared with a simulation using the Geophysical Fluid Dynamics Laboratory operational hurricane model (Möller and Shapiro, 2002). In contrast, our calculations show the opposite result: the balanced tendency underestimates the tendency in MM5 by a factor of two in the eyewall. Nevertheless, our results are in agreement with Möller and Shapiro in that the balanced calculation significantly underestimates the tendency in MM5 in the boundary layer. We would argue that the underestimate of the intensification rate by the balanced solution in the eyewall is to be expected in a rapidly intensifying storm as the time-scale for the VHTs is short compared with the evolution time-scale of the system-scale vortex.

5.1. Spin-up of the outer circulation

In M3 it was argued that the spin-up of the outer circulation is due to the radial convergence above the boundary layer in the presence of absolute angular momentum conservation and that this spin-up process should be largely captured by axisymmetric balance dynamics. To check this, we show in Figure 10(a) vertical profiles of the tangential wind tendency estimated from the radial influx of absolute vorticity (the first term on the right-hand side of Equation (18)) at radii of 150, 175, 200 and 249 km. The large tendency values below about 1 km will be mostly opposed by the negative tendency of friction. The tendencies are significantly larger in the MM5 calculation on account of the larger inflow therein compared with the balanced calculation (e.g. Figure 10(b)). Above this level, values are mostly on the order of $0.05–0.4$ m s^{-1} h^{-1} in both sets of calculations, but they are noticeably larger in the balanced calculation, a fact that may be attributed to larger radial flow above the boundary layer in this calculation. The agreement above the boundary layer is much improved if we compare the balanced calculation with that based on a 2 h average of the 15 min MM5 output, shown also in Figure 10. The reason is that the instantaneous velocities in MM5 contain inertia-gravity waves, the effects of which are reduced by averaging. Note that the balanced calculation captures the averaged lower-tropospheric inflow rather well at 200 km radius (Figure 10(b)).

The foregoing results confirm the statement made in M3 that the progressive growth in the vortex size can be attributed to inflow above the boundary layer induced by convective heating and that this inflow can be explained largely on the basis of balance dynamics.
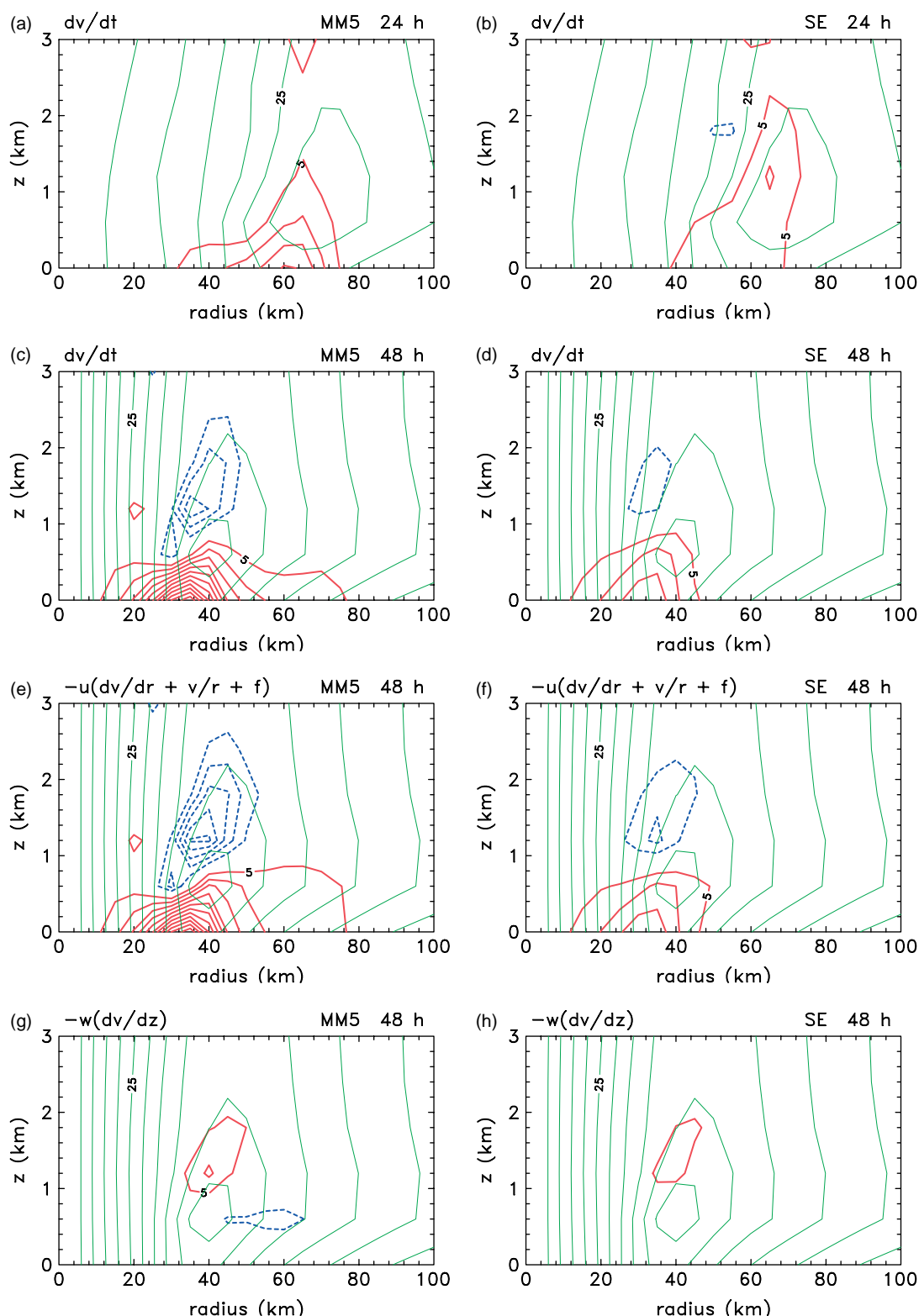
Figure 9. Radius–height cross-sections of the azimuthally–averaged tangential wind tendency, $\partial v/\partial t$, at low altitude in the inner-core region at 24 h calculated from (a) the MM5 solution, and (b) the balanced solution (SE). (c) and (d) show the corresponding plots at 48 h. (e) and (f) show the contributions to the tendency at 48 h in (c) and (d) from the horizontal influx of absolute vorticity (the term $-u(\partial v\partial r + v/r + f)$ in Equation (18)). (g) and (h) show the corresponding contributions from the vertical advection of tangential momentum (the term $-w\partial v/\partial z$ in Equation (18)). The tendencies have a contour interval of 5 m s^{-1}h^{-1} (solid for positive and dashed for negative). All panels show also the isotachs (thin lines) of tangential wind with interval 5 m s^{-1}. This figure is available in colour online at www.interscience.wiley.com/journal/qj
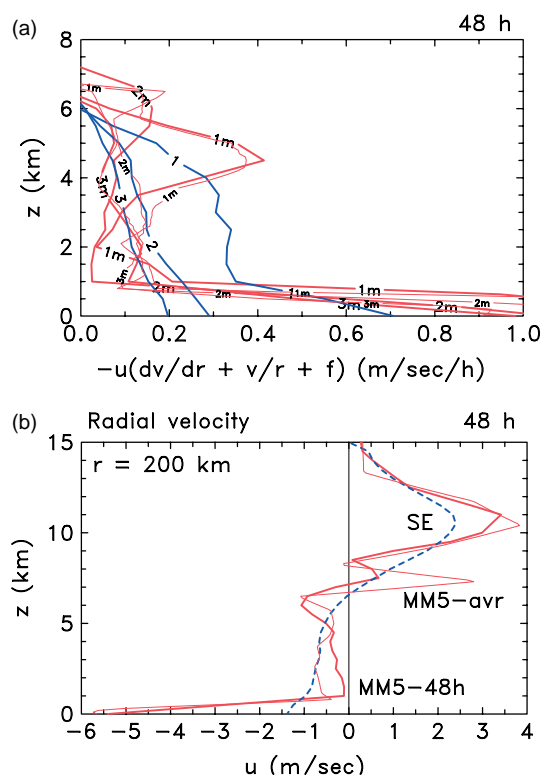
Figure 10. (a) Vertical profiles of the azimuthally–averaged tangential wind tendency estimated from the radial advection of absolute vorticity (the first term on the right-hand side of Equation (18)) at radii of 150 km (curves labelled 1), 200 km (curves labelled 2), and 249 km (curves labelled 3) at 48 h from the MM5 (suffix m) and SE calculation. (b) Vertical profiles of the radial wind component at a radius of 200 km at this time (solid curves for MM5, dashed curve for SE). The thin curves in (a) show the radial advective tendency, and in (b) the radial velocity, when the MM5 fields are averaged at 15 min intervals between 47 and 49 h. Note that the ordinate scales in these two panels are different. This figure is available in colour online at www.interscience.wiley.com/journal/qj

5.2. Regularized versus non-regularized SE calculations

Figure 11 shows radius–height cross-sections of the streamfunction, the radial wind component, the vertical velocity, and the azimuthally–averaged tangential wind tendency, $\partial v/\partial t$, derived from the solution of the SE equation at 48 h in the case where the regularization procedure described in section 4 is not applied. Without the regularization procedure, the streamfunction field is markedly stronger than in the solution of the regularized SE equation (cf. Figures 11(a) and (b)) and therefore the radial and vertical components of flow are stronger also (cf. Figures 11(b) and (c) with 6(b) and 7(b), respectively), bringing them closer to the MM5 solution. Now the radial flow exhibits shallow regions of inflow or reduced outflow in the upper troposphere, much like that in the the MM5 calculation (Figure 6(a)). We attribute this structure to the presence of the symmetrically unstable region indicated in Figure 2(b). In contrast, the tangential wind tendency in the non-regularized SE calculation is close to that of the regularized solution, a consequence of the fact that the largest spin-up occurs at low levels in the inner-core region, remote from the regions of inertial instability. Thus, despite the fact that the SE equation is

solved globally, the flow at radii less than about 70 km is similar in the solutions with and without regularization. The comparison strongly suggests that the shallow region of inflow in the upper troposphere in the MM5 solution is a consequence of inertial instability.

Even though it is possible to obtain a solution when the SE equation is not regularized, the solution in this case is sensitive to the vertical resolution, presumably a reflection of the well-known property that (linear) symmetric instability seeks structures with a small vertical scale. This feature has an analogue in the case of buoyant instability, where small horizontal scales are favoured.

6. Conclusions

We have examined the balanced axisymmetric dynamics of a hurricane in the framework of an idealized three-dimensional non-hydrostatic numerical model simulation. Specifically we have investigated the degree to which the azimuthally–averaged fields in the simulation deviate from those which are diagnosed assuming gradient wind balance. The procedure was to use the azimuthally–averaged diabatic heating rate and tangential momentum source diagnosed from the simulation as forcing functions for the Sawyer–Eliassen equation. The secondary circulation obtained by solving this equation was compared with that deduced at selected times from an azimuthal average of the three-dimensional simulation. The principal findings can be summarized as follows.

The balanced calculation captures a major fraction of the azimuthally–averaged secondary circulation of the three-dimensional simulation except in the boundary layer, where the balanced assumption breaks down and where there is an inward agradient force. In this layer, the balanced calculation underestimates the strength of the inflow, but it largely compensates for this underestimate by overestimating the inflow in the lower troposphere above the boundary layer. As a result, the maximum vertical velocity is only marginally stronger in the MM5 calculation. The updraught in the balanced calculation does not extend quite so high as in the MM5 calculation, a result that is presumably a consequence of the inability of the balance theory to represent the local buoyancy forces within the VHTs, which have been shown previously to be a fundamental aspect of the dynamics in the three-dimensional simulation.

In the balance theory, the diabatic forcing associated with the eyewall convection accounts for a large fraction of the secondary circulation. It negates the divergence above the boundary layer that would be produced by friction alone. In particular, diabatic heating induces radial inflow, both within and above the boundary layer.

The balanced solution considerably underestimates the intensification rate in the boundary layer. This result is a reflection of the inability of the balanced calculation to fully capture the dynamics of the boundary layer in the inner core region and, in particular, the strength of the inflow there.
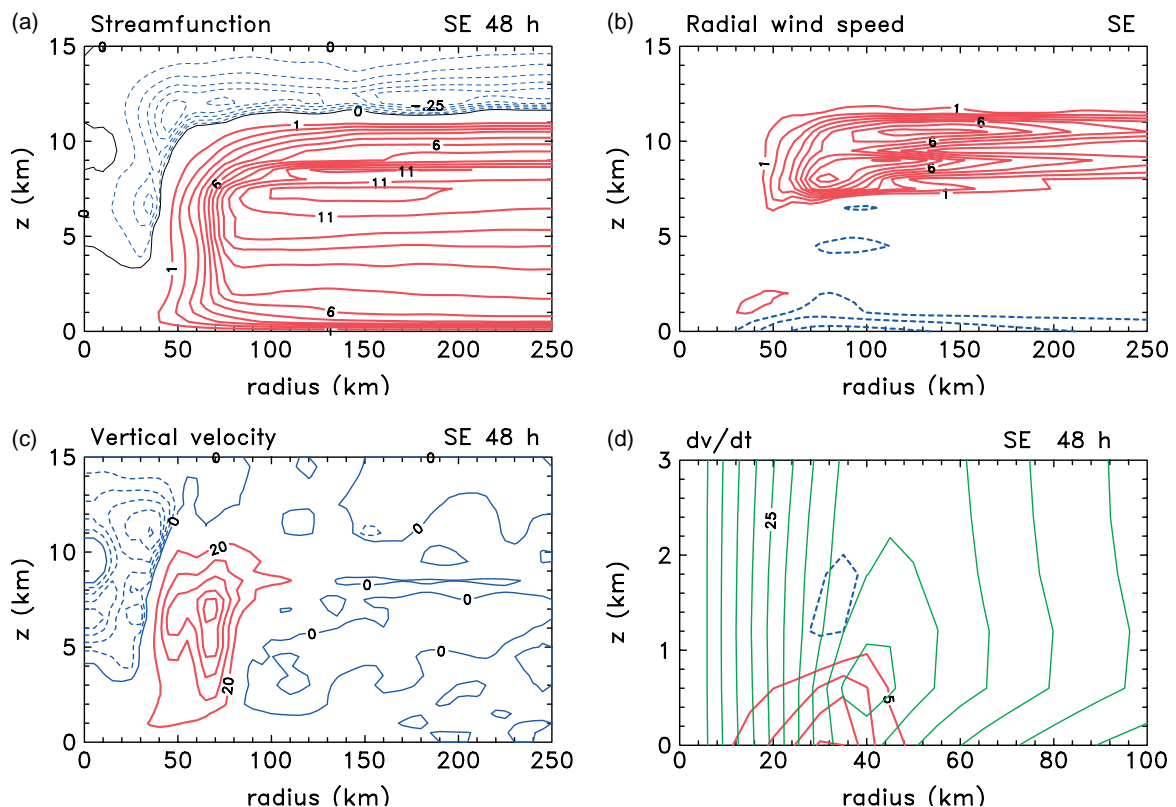
Figure 11. Radius–height cross-sections of (a) the streamfunction, (b) the azimuthally–averaged radial wind component, (c) the azimuthally–averaged vertical velocity, and (d) the azimuthally–averaged tangential wind tendency, $\partial v/\partial t$, derived from the solution of the SE equation at 48 h in the case where the regularization procedure described in section 4 is not applied. These fields should be compared with those for the regularized SE solution shown in Figures 4(b), 6(b), 7(b), and 9(d), respectively. Contour intervals are the same as in the latter figures, except the thick dashed contours in (d) have a contour interval twice that of the solid contours. It is important to note that the domain of (d) is only a small part of that shown in the other panels. This figure is available in colour online at www.interscience.wiley.com/journal/qj

In contrast to an earlier study, we have found that the balanced solution underestimates the intensification rate in the eyewall as well. We would argue that this underestimate is to be expected in a rapidly intensifying storm as the balance approximation assumes that the vortex evolves on a time-scale that is slow compared with the intrinsic frequencies of oscillation of the vortex. The VHTs, which are driving the intensification process, project strongly onto these frequencies and it is therefore not surprising that the balanced solution effectively lags behind the true state. In the light of this result, it *is* surprising how well the balanced calculation captures the principal features of the secondary circulation.

The progressive growth in the outer swirling circulation of the vortex in the MM5 model can be attributed to inflow above the boundary layer induced by convective heating in the eyewall. This inflow can be explained largely on the basis of balance dynamics.

Because of the development of regions of symmetric instability in the numerical model calculations, it is necessary to regularize the Sawyer–Eliassen equation. A procedure for accomplishing this regularization was described. It is still possible to obtain a solution of the Sawyer–Eliassen equation without a regularization, but the solution is then dependent on the vertical resolution used for the calculation.

A consequence of symmetric instability is the appearance of a shallow layer (or layers) of inflow or reduced outflow in the upper troposphere, both in the three-dimensional model and in the non-regularized balanced solutions.

Balance dynamics continue to provide essential insight in geophysical vortex dynamics. The findings herein affirm the utility of these ideas even in understanding basic aspects of vortex intensification in a three-dimensional, non-hydrostatic model. This work highlights the lower tropospheric regions in which the balance assumption breaks down and examines the consequences of this breakdown during rapid intensification.

Acknowledgements
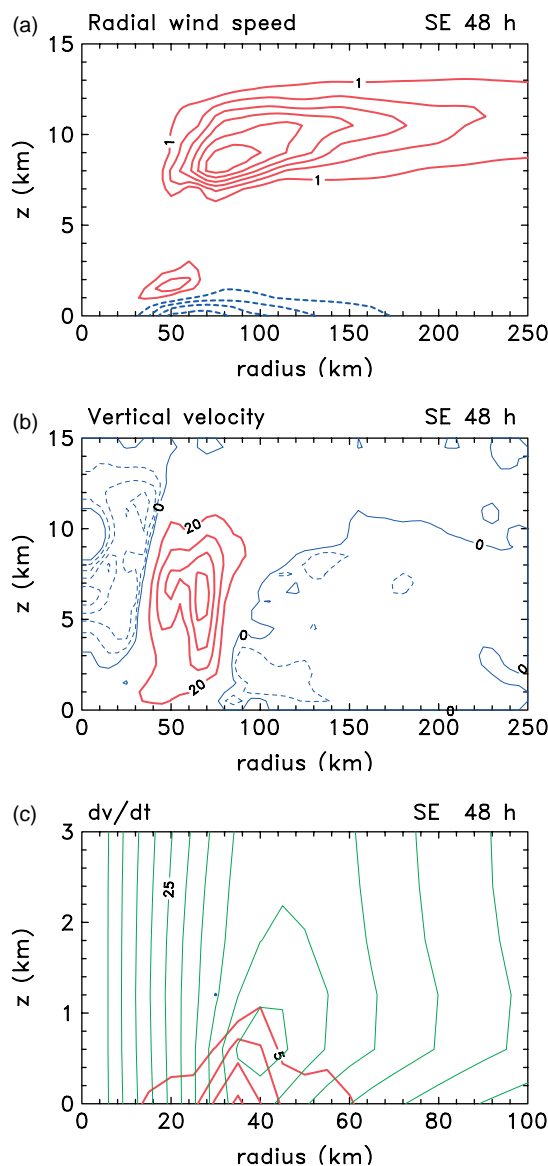
H. H. BUI *ET AL.*

Figure 12. Radius–height cross-sections of (a) the azimuthally–averaged radial wind component, (b) the azimuthally–averaged vertical velocity, and (c) the azimuthally–averaged tangential wind tendency, $\partial v/\partial t$, derived from the solution of the SE equation at 48 h in the case where the azimuthally–averaged temperature field is taken directly from the MM5 solution and is not accurately in balance with the azimuthally–averaged tangential wind component. The thin curves in (c) show the azimuthally–averaged tangential wind component at this time. These panels should be compared with Figures 6(b), 7(b) and 9(d), respectively. The contour intervals are the same as in these corresponding figures. This figure is available in colour online at www.interscience.wiley.com/journal/qj

Appendix

The consequences of using a balanced temperature field

As far as we are aware, most previous studies that use the balanced framework for diagnosing the secondary circulation in models have used model-derived azimuthally–averaged azimuthal wind and temperature fields to calculate the parameters in the SE equation, even though these fields may not satisfy gradient- or thermal-wind balance exactly. The question arises: how important

is the lack of balance in solving the SE equation? We investigate this question below.

We show first that the lack of balance effectively introduces an implicit forcing term on the right-hand side of the SE equation. For simplicity we examine the Boussinesq case outlined in section 2 and assume that hydrostatic balance expressed by Equation (3) is accurately satisfied. We may write Equation (1) in the form:

$$ C - \frac{\partial P}{\partial r} = \dot{U}, \tag{A1} $$

where $\dot{U}$ quantifies the degree of gradient wind balance. The analysis outlined in section 2 proceeds in a similar way, but now the thermal wind Equation (7) has the form

$$ \frac{\partial b}{\partial r} = \xi \frac{\partial v}{\partial z} - \frac{\partial \dot{U}}{\partial z}. \tag{A2} $$

Now, when this equation is differentiated partially with respect to time, there is an additional term $\partial^2 \dot{U}/\partial t \partial z$ from which the time derivative cannot be eliminated as before. This term will appear as a time-dependent forcing term on the right-hand side of the SE equation. Obviously the balanced diagnostic approach then breaks down. In principle, one could calculate the spatial distribution of this term from the results of the numerical model simulation and solve the SE equation with it included. However, to quantify the possible importance of the lack of balance, it is simpler to compare the solution obtained using a balanced temperature field with one using the model-derived azimuthally–averaged temperature field.

Figure 12 compares the radial wind components and the azimuthal wind tendencies at 48 h obtained from the two methods. The most significant differences are in the radial wind fields, the low-level inflow being twice as strong in the calculation with azimuthally–averaged temperature field. However, the outflow near radii where the inflow terminates is stronger also so that the vertical velocity in the two calculations is much the same. Despite the stronger inflow, the tendencies are almost the same in the two calculations, the reason being that the stronger winds are not colocated with the radius of the maximum absolute vorticity, which at 48 h is only 10 km.

References

Bell MM, Montgomery MT. 2008. Observed structure, evolution, and potential intensity of category 5 hurricane *Isabel* (2003) from 12 to 14 September. *Mon. Weather Rev.* **65**: 2025–2046.

Challa M, Pfeffer RL. 1980. Effects of eddy fluxes of angular momentum on model hurricane development. *J. Atmos. Sci.* **37**: 1603–1618.

Emanuel KA. 1986. An air-sea interaction theory for tropical cyclones. Part I: Steady state maintenance. *J. Atmos. Sci.* **43**: 585–604.

Emanuel KA. 1989. The finite amplitude nature of tropical cyclogenesis. *J. Atmos. Sci.* **46**: 3431–3456.

Emanuel KA. 1995a. Sensitivity of tropical cyclones to surface exchange coefficients and a revised steady-state model incorporating eye dynamics. *J. Atmos. Sci.* **52**: 3969–3976.

Emanuel KA. 1995b. The behavior of a simple hurricane model using a convective scheme based on subcloud-layer entropy equilibrium. *J. Atmos. Sci.* **52**: 3960–3968.

Emanuel KA. 1997. Some aspects of hurricane inner-core dynamics and energetics. *J. Atmos. Sci.* **54**: 1014–1026.

Emanuel KA. 2003. Tropical cyclones. *Annu. Rev. Earth Planet. Sci.* **31**: 75–104.

Hendricks EA, Montgomery MT, Davis CA. 2004. On the role of 'vortical' hot towers in formation of tropical cyclone Diana (1984). *J. Atmos. Sci.* **61**: 1209–1232.

Möller JD, Shapiro L. 2002. Balanced contributions to the intensification of hurricane *Opal* as diagnosed from a GFDL model forecast. *Mon. Weather Rev.* **130**: 1866–1881.

Möller JD, Smith RK. 1994. The development of potential vorticity in a hurricane-like vortex. *Q. J. R. Meteorol. Soc.* **120**: 1255–1265.

Montgomery MT, Kallenbach R. 1997. A theory for vortex-Rossby waves and its application to spiral bands and intensity changes in hurricanes. *Q. J. R. Meteorol. Soc.* **123**: 435–465.

Montgomery MT, Nguyen SV, Smith RK. 2009. Do tropical cyclones intensify by WISHE? *Q. J. R. Meteorol. Soc. in press.*

Montgomery MT, Nicholls ME, Cram TA, Saunders AB. 2006. A vortical hot tower route to tropical cyclogenesis. *J. Atmos. Sci.* **63**: 355–386.

Nguyen SV, Smith RK, Montgomery MT. 2008. Tropical cyclone intensification and predictability in three dimensions. *Q. J. R. Meteorol. Soc.* **134**: 563–582.

Ogura Y, Phillips NA. 1962. Scale analysis of deep and shallow convection in the atmosphere. *J. Atmos. Sci.* **19**: 173–179.

Ooyama KV. 1969. Numerical simulation of the life cycle of tropical cyclones. *J. Atmos. Sci.* **26**: 3–40.

Persing J, Montgomery MT. 2003. Hurricane superintensity. *J. Atmos. Sci.* **60**: 2349–2371.

Persing J, Montgomery MT, Tuleya RE. 2002. Environmental interactions in the GFDL hurricane model for hurricane *Opal*. *Mon. Weather Rev.* **130**: 298–317.

Pfeffer RL, Challa M. 1981. A numerical study of the role of eddy fluxes of momentum in the development of Atlantic hurricanes. *J. Atmos. Sci.* **38**: 2393–2398.

Press WH, Teukolsky SA, Vetterling WT, Flannery BP. 1992. *Numerical Recipes in C: The art of scientific computing.* Cambridge University Press: Cambridge, UK.

Schubert WH, Alworth BT. 1987. Evolution of potential vorticity in tropical cyclones. *Q. J. R. Meteorol. Soc.* **113**: 147–162.

Schubert WH, Hack JJ. 1983. Transformed Eliassen balanced vortex model. *J. Atmos. Sci.* **40**: 1571–1583.

Schubert WH, Rozoff CM, Vigh JL, McNoldy BD, Kossin JP. 2007. On the distribution of subsidence in the hurricane eye. *Q. J. R. Meteorol. Soc.* **133**: 1–20.

Shapiro LJ, Montgomery MT. 1993. A three-dimensional balance theory for rapidly rotating vortices. *J. Atmos. Sci.* **50**: 3322–3335.

Shapiro LJ, Willoughby H. 1982. The response of balanced hurricanes to local sources of heat and momentum. *J. Atmos. Sci.* **39**: 378–394.

Shin S, Smith RK. 2008. Tropical cyclone intensification and predictability in a minimal three-dimensional model. *Q. J. R. Meteorol. Soc.* **134**: 1661–1671.

Smith RK. 1980. Tropical cyclone eye dynamics. *J. Atmos. Sci.* **37**: 1227–1232.

Smith RK. 2000. The role of cumulus convection in hurricanes and its representation in hurricane models. *Rev. Geophys.* **38**: 465–489.

Smith RK. 2006. Accurate determination of a balanced axisymmetric vortex. *Tellus* **58A**: 98–103.

Smith RK, Montgomery MT. 2008. Balanced boundary layers in hurricane models. *Q. J. R. Meteorol. Soc.* **134**: 1385–1395.

Smith RK, Montgomery MT, Nguyen SV. 2009. Tropical cyclone spin-up revisited. *Q. J. R. Meteorol. Soc.* **135**: 1321–1335.

Smith RK, Montgomery MT, Zhu H. 2005. Buoyancy in tropical cyclones and other rapidly rotating vortices. *Dyn. Atmos. Oceans* **40**: 189–208.

Sundqvist H. 1970. Numerical simulation of the development of tropical cyclones with a ten-level model. Part I. *Tellus* **22**: 359–389.

Willoughby HE. 1979. Forced secondary circulations in hurricanes. *J. Geophys. Res.* **84**: 3173–3183.

Willoughby HE. 1990. Gradient balance in tropical cyclones. *J. Atmos. Sci.* **47**: 465–489.

Zhang D-L, Liu Y, Yau MK. 2001. A multi-scale numerical study of hurricane *Andrew* (1992). Part IV: Unbalanced flows. *Mon. Weather Rev.* **129**: 92–107.